Quantum manifestation of a synchronization transition in optomechanical systems

Lei Ying,[1] Ying-Cheng Lai,[1,2,3,*] and Celso Grebogi[3]
[1]*School of Electrical, Computer, and Energy Engineering, Arizona State University, Tempe, Arizona 85287, USA*
[2]*Department of Physics, Arizona State University, Tempe, Arizona 85287, USA*
[3]*Institute for Complex Systems and Mathematical Biology, King's College, University of Aberdeen, Aberdeen AB24 3UE, United Kingdom*
(Received 14 August 2014; published 5 November 2014)

Recent years have witnessed significant interest in nanoscale physical systems, such as nanoelectromechanical and optomechanical systems, which can exhibit distinct collective dynamical behaviors, such as synchronization. As a parameter of the system changes, transition from one type of emerging collective behavior to another can occur. But what are the quantum manifestations of such a transition? We investigate a system of two optically coupled optomechanical cavities and uncover the phenomenon of transition from in-phase to antiphase synchronization. Quantum mechanically, we find that, associated with the classical transition, the entanglement measures between the various optical and mechanical degrees of freedom in the two cavities exhibit a change characteristic of second-order phase transition. These phenomena can be tested experimentally.

DOI: 10.1103/PhysRevA.90.053810 PACS number(s): 42.65.Sf, 05.45.Mt, 03.65.Ud

A fundamental and important problem in physics is the understanding of the quantum manifestations of classical nonlinear and complex dynamical behaviors. In this regard, the field of quantum chaos aims to uncover and exploit the various quantum phenomena in systems exhibiting chaos in the classical limit [1]. There is now a large body of literature on quantum chaos, but most works in this field focused on classical Hamiltonian systems of relatively low dimensions, addressing issues such as energy level-spacing statistics [2], quantum scarring [3], and quantum chaotic scattering [4].

The phase space dimension of complex dynamical systems can be rather high due to the number of interacting components. A higher-level description characterizing the mutual relations among the components and the emerging collective behaviors then becomes highly relevant. There are distinct types of collective dynamics in complex systems, such as synchronization [5] and antiphase synchronization [6]. In micro- and nanoscale systems, there is growing interest in exploiting synchronization [7] for significant applications. For example, phase locking in a pair of mechanically coupled nano-beams was demonstrated [8], and the idea of using optical coupling to synchronize micromechanical oscillators was exploited [9,10] for potential application in realizing massive optomechanical oscillator arrays [11]. Recent years have also witnessed growing interest in the quantum manifestations of *classical collective dynamics*, such as quantum synchronization [12] and entanglement of qubits coupled to a driven dissipative resonator [13], quantum synchronization of van der Pol oscillators with trapped ions [14], quantum-classical transition of correlations of two coupled cavities [15], quantum many-body dynamics in optomechanical arrays [16], and entanglement tongue and quantum synchronization of disordered oscillators [17].

In physics, various transition phenomena induced by changes in system parameters are basic and relevant. Examples are phase transitions in statistical physics and bifurcations to distinct dynamical states including chaos. Suppose the complex system of interest exhibits a transition from one type of collective dynamical behavior to another, and further assume that quantum effects cannot be neglected (e.g., for a nanoscale system). What are the quantum manifestations of the transition? To address this general question in a concrete setting, we consider a class of physical systems of considerable recent interest: optomechanical systems [18–22].

A single optomechanical system consists of an optical cavity and a nanoscale mechanical oscillator, typically a cantilever. When a laser beam is introduced into the cavity, a resonant optical field emerges, exerting a radiation force on the mechanical cantilever, causing it to oscillate. The mechanical oscillations in turn change the length of the optical cavity, hence its resonant frequency. There is thus a coupling between the optical and mechanical degrees of freedom. This coupling, or interaction, can in fact lead to the cooling of the mechanical oscillator, a subject of intense recent research [23]. Here, we consider the setting of two optomechanical subsystems mutually coupled through an optical fiber [24], as shown in Fig. 1. Both subsystems are driven by a common driving laser beam. This photon-photon coupling scheme is experimentally realizable, e.g., through two coupled optical fiber taper waveguides [10,25]. A generalized version of our system is a crystal structure of a series of mutually coupled optomechanical subsystems, which has many potential applications [9,10,21,22]. Utilizing the Heisenberg equations of motion, we describe each optomechanical subsystem by a set of nonlinear equations of four dynamical variables in the phase space: the real and complex components of the optical field, and the position and velocity of the mechanical cantilever. The classical phase space dimension of the coupled optomechanical system is thus eight. In our analysis, synchronization occurs when the normalized power λ of the common driving laser is relatively low. But as λ is increased through a critical point λ_c, a transition to antiphase synchronization occurs, this being a novel phenomenon in optomechanics that can be tested experimentally with potential applications in integrated optomechanical systems [19]. To uncover the quantum manifestations of the transition, we study and pay particular attention to quantum entanglement between the two coupled optomechanical subsystems. Calculation of the entanglement measures [20] associated with various optical and mechanical degrees of freedom reveals a distinct type of

*ying-cheng.lai@asu.edu

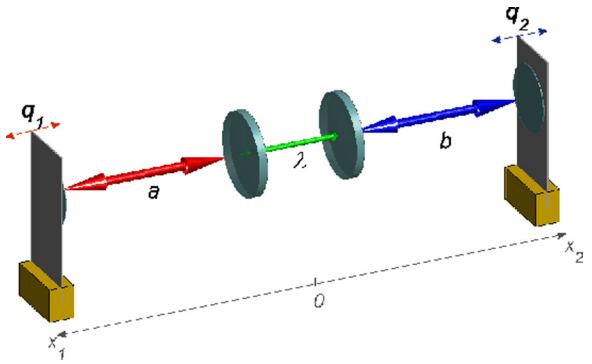

FIG. 1. (Color online) Schematic illustration of our system of two coupled optomechanical cavities. The coupling between the two subsystems is realized by an optical fiber with λ being the coupling parameter. The displacements of the cantilevers are denoted by $q_{1,2}$.

quantum manifestation of the synchronization transition: As the transition point is crossed, the maximum entanglement measure is continuous but its derivative with respect to the parameter λ is discontinuous. This is characteristic of a second-order phase transition. In spite of the recent works on quantum synchronization, the second-order nature of the quantum change associated with transition in the classical collective dynamics has not been identified before. Since it is not necessary to drive the individual optomechanical subsystems into highly nonlinear regimes for the synchronization transition to occur, it is feasible to test our findings experimentally.

We consider two identical optomechanical subsystems coupled through an optical fiber [24], as shown in Fig. 1. Each individual system is a Fabry-Perot cavity with one fixed and one movable mirror. We assume that there is only one photon mode with frequency $\omega = 2\pi c/L$, where L is the length of each cavity. The Hamiltonian of the whole coupled system can be divided into three parts: $H = H_a + H_b + H_c$. The sub-Hamiltonians $H_{a(b)}$ describe the individual subsystems. We have $H_a + H_b = \Delta_0(a^\dagger a + b^\dagger b) + (\omega_m/2)[(p_1^2 + q_1^2) + (p_2^2 + q_2^2)] + G_0(a^\dagger a q_1 + b^\dagger b q_2)$, where $a^\dagger(b^\dagger)$ and $a(b)$ are the creation and annihilation operators, respectively. The first and second terms of $H_a + H_b$ describe the cavity and mechanical modes, respectively, and the last term represents the nonlinear coupling between the optical and mechanical modes in each subsystem caused by the radiated pressure. The coupling between the two subsystems is linear, which can be described by the Hamiltonian $H_c = \lambda(a^\dagger b + b^\dagger a)$, where λ is the optical coupling strength. The dynamics of the coupled system are governed by the quantum Langevin equations [19]: $\partial\hat{O}/\partial t = i[\hat{H}, \hat{O}] + \hat{N} - \hat{H}_{\rm diss}$, where $\hat{N}$ is the quantum fluctuation operator, $\hat{H}_{\rm diss}$ characterizes the dissipation, and $\hat{O} = p_1, q_1, a$ denotes the operators for the left cavity and p_2, q_2, b for the right cavity, where $p_{1,2} = \omega_m \dot{q}_{1,2}$. The set of quantum Langevin equations is then given by

$$\begin{aligned}
\dot{p}_1 &= -\omega_m q_1 + G_0 a^\dagger a - \gamma_m p_1 + \xi_1, \\
\dot{a} &= -(\kappa + i\Delta_0)a + iG_0 a q_1 + E - i\lambda b + \sqrt{2\kappa}a^{in}, \\
\dot{p}_2 &= -\omega_m q_2 + G_0 b^\dagger b - \gamma_m p_2 + \xi_2, \\
\dot{b} &= -(\kappa + i\Delta_0)b + iG_0 b q_2 + E - i\lambda a + \sqrt{2\kappa}b^{in}, \quad (1)
\end{aligned}$$

where κ is the decay rate of each cavity, γ_m is the mechanical damping rate, and the laser detuning is given by $\Delta_0 = \omega_c - \omega_0$. Here ω_c and ω_0 are, respectively, the frequencies of the cavity mode and of the driving laser, and $E = E_0 + E_1 \cos(\Omega t)$ is the driven external field. The driven frequency is $\Omega = 2\omega_m$. The vacuum radiation input noise a^{in} and (b^{in}) are stochastic processes [26] described by $\langle a^{in}(t)a^{in,\dagger}(t')\rangle = \langle b^{in}(t)b^{in,\dagger}(t')\rangle = \delta(t - t')$, and the Hermitian Brownian noise operator is characterized by its autocorrelation function, in the Markovian approximation [27], as $\langle \xi_{1,2}(t)\xi_{1,2}(t') + \xi_{1,2}(t')\xi_{1,2}(t)\rangle/2 = \gamma_m(2\bar{n} + 1)\delta(t - t')$, where $\bar{n} = 1/[\exp(\hbar\omega_m/k_B T) - 1]$. The mechanical and optical noise operators have zero mean values.

To uncover the transitions in the classical dynamics, we solve the deterministic version of the quantum Langevin equations without the noise terms in Eq. (1), for the following experimental parameter setting [18,21,22,28]: $L = 25$ mm, $F = 1.4 \times 10^4$, $\omega_m = 2\pi \times 10^6$ Hz, $Q = 10^6$, and $m = 150$ ng. We use a red detuned laser ($\Delta_0 \simeq \omega_m$) with wavelength $\lambda = 1064$ nm. The modulation coefficients E_n ($n = 0, \pm 1$) in Eq. (1) are given by $E_n = \sqrt{2\kappa P_n/(\hbar\omega_o)}$ with the power of the associated sidebands $P_0 = 10 \times 10^{-3}$W and $P_{\pm 1} = 0.5 \times 10^{-3}$W, where the decay rate is $\kappa = \pi c/(2FL)$ (c being the speed of light). In the computation, we normalize the above parameters by ω_m, so we have $\gamma_m/\omega_m = 1 \times 10^{-6}$, $G_0/\omega_m = 3.7726 \times 10^{-6}$, $\Delta_0/\omega_m = 1$, $\kappa/\omega_m = 0.107$, $E_0/\omega_m = 6.042 \times 10^4$, $E_1/\omega_m = 1.351 \times 10^4$, and $\Omega/\omega_m = 2$. (For calculation of the quantum entanglement measure to be described below, we set $\bar{n} = 0.05$.) We find that, as the coupling parameter λ is increased through a critical value $\lambda_c \approx 0.39082$, there is a transition from in-phase to antiphase synchronization. Figures 2(a)–2(f) show the time evolution of various dynamical variables for two different values of λ: one before the transition ($\lambda = 0.388$, left column) and another after the transition ($\lambda = 0.398$, right column). We observe that, in the synchronized (in-phase, left column) state, the system exhibits limit-cycle oscillations. In the antiphase synchronization state (right column), the system exhibits period-2 oscillations.

To understand the transition from synchronization to antiphase synchronization, we plot the bifurcation diagrams of various dynamical variables versus the coupling parameter λ, as shown in Fig. 3(a), where the red and green curves correspond to peak and valley values of the real and imaginary parts of the photon operator a and b, respectively. We observe a Hopf bifurcation at the transition point. The bifurcation behavior of the mechanical operator $q_{1(2)}$ appears slightly more complicated than that associated with the optical operator. On both sides of the critical point λ_c, each mechanical variable has two branches, but the oscillation amplitude becomes larger as λ is increased through λ_c. The black dashed curves indicate the behaviors of the unstable oscillations about λ_c, whose amplitudes remain unchanged through the transition. Note that, in the real quantum system, due to existence of noise, the unstable state, as well as continuation of steady state before critical point, would disappear. Also shown in Fig. 3(a) are the basin structures. In particular, for $\lambda < \lambda_c$, the in-phase synchronized state is the only stable state in the system but it becomes unstable for $\lambda > \lambda_c$, where antiphase

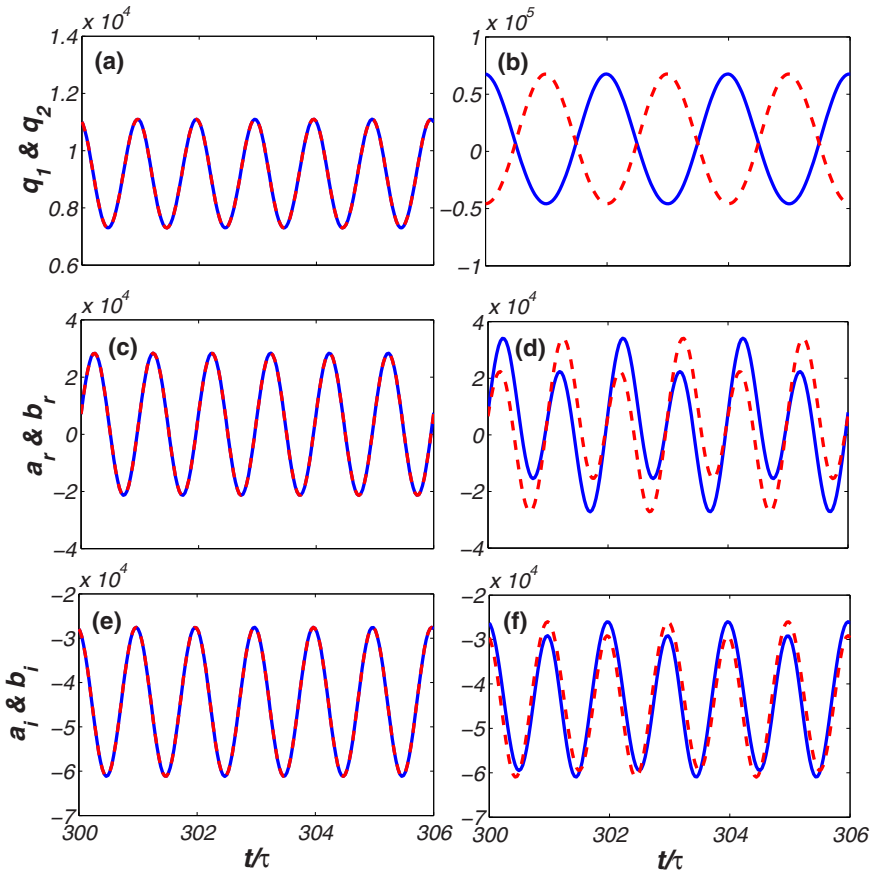

FIG. 2. (Color online) (a) and (b) Time evolution of the mechanical operators $\hat{q}_{1(2)}$, and (c) and (d) the real, and (e) and (f) imaginary parts of the optical operators $\hat{a}(\hat{b})$. There is a transition from synchronization to antiphase synchronization as the coupling parameter λ passes through the critical point $\lambda_c \approx 0.39082$. The left and right columns correspond to $\lambda = 0.388$ (before the transition) and 0.398 (after the transition), respectively. Note that there is a phase difference π in all panels in the right column. Especially, for (d) and (f), the optical fields exhibit a period-2 behavior. A π phase shift will make the solid and dashed traces overlap with each other completely.

synchronization state becomes stable. Figure 3(b) shows a magnification of the bifurcation diagram of the mechanical variables. As shown schematically in Fig. 3(c), the bifurcation at λ_c can be understood as a continuation of the modulation due to the driven optical field and the occurrence of a standard Hopf bifurcation at λ_c superimposed on the original oscillations. Since the frequencies of the driven optical field and the limit-cycle oscillations generated by the Hopf bifurcation are incommensurate, the combination of the two leads to period-2 oscillations in both cavities but with the phase difference of π. The bifurcation at λ_c is thus *not* a period doubling bifurcation.

The stabilities of the collective motions about the transition point can be characterized by the transverse Lyapunov exponents (TLEs) [29]. As shown in Fig. 3(d), the largest nontrivial TLE associated with the synchronized state is negative before the transition but it becomes positive after the transition. The synchronized state is thus stable for $\lambda < \lambda_c$ but it is unstable for $\lambda > \lambda_c$. At the transition, where the antiphase synchronization state is born, its largest nontrivial TLE is zero but decreases linearly past the transition point. The antiphase synchronization state is thus stable for $\lambda > \lambda_c$.

To characterize the quantum manifestation of the collective transition at λ_c, we measure the degree of quantum entanglement, which is defined as the logarithmic negativity (LN) [30]. It can be calculated through the covariance matrix $V(t)$ whose time evolution is governed by [28]

$$dV(t)/dt = A(t)V(t) + V(t)A^T(t) + D, \qquad (2)$$

where $D = \mathrm{diag}[0, \gamma_m(2\bar{n}+1), \kappa, \kappa, 0, \gamma_m(2\bar{n}+1), \kappa, \kappa]$, and the matrix A is

$$A = \begin{bmatrix} A_1 & A_c \\ A_c & A_2 \end{bmatrix}, \qquad (3)$$

with

$$A_{1,2} = \begin{bmatrix} 0 & \omega_m & 0 & 0 \\ -\omega_m & -\gamma_m & \mathrm{Re}(G_{a,b}) & \mathrm{Im}(G_{a,b}) \\ -\mathrm{Im}(G_{a,b}) & 0 & -\kappa & \Delta_{a,b} \\ \mathrm{Re}(G_{a,b}) & 0 & -\Delta_{a,b} & -\kappa \end{bmatrix}, \qquad (4)$$

and

$$A_c = \begin{bmatrix} 0 & 0 & 0 & 0 \\ 0 & 0 & 0 & 0 \\ 0 & 0 & 0 & \lambda \\ 0 & 0 & -\lambda & 0 \end{bmatrix}. \qquad (5)$$

The matrix elements are written as $G_{a,b} = \sqrt{2}G_0\langle a, b(t)\rangle$ and $\Delta_{a,b} = \Delta_0 - G_0\langle q_{1,2}(t)\rangle$. The elements of the covariance matrix $V(t)$ at one time step are given by $V_{ij} = \langle u_i u_j + u_j u_i\rangle/2$, where $u_i = \delta O_i = O_i - O_i^s$ with $O_i = q_1, p_1, a_r, a_i, q_2, p_2, b_r$ or b_i and the upper index "s" stands for "stable state." For our coupled optomechanical system, the covariance matrix contains information about quantum entanglement among two mechanical and two optical modes; thus its size is 8×8. The

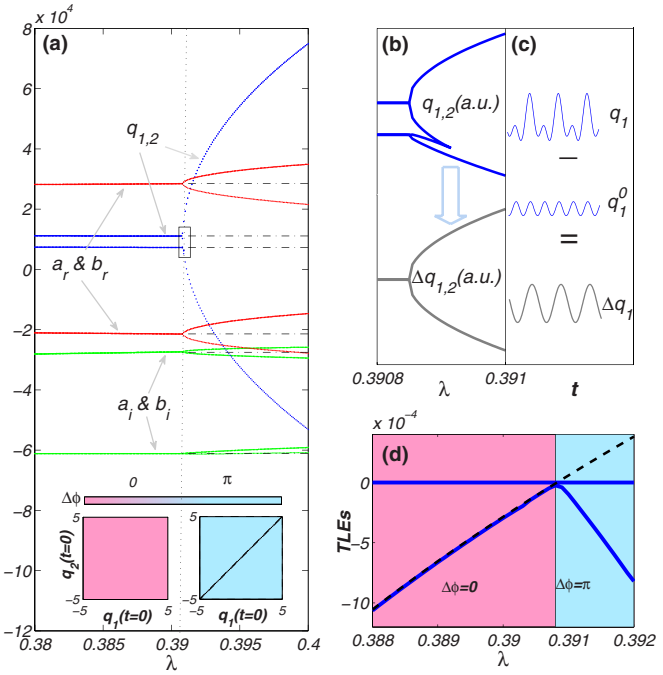

FIG. 3. (Color online) (a) Bifurcation diagrams for the mechanical variables ($q_{1,2}$, blue curve), the real (a_r and b_r, red curves), and imaginary parts of the cavity operators (a_i and b_i, green curves). The black dashed lines indicate the unstable state after the transition. The basin structures before and after the synchronization transition are also shown, where the pink and light blue areas correspond to the in-phase and antiphase synchronization states, respectively. (b) and (c) Extraction of Hopf bifurcation at the transition point, where q_1 and q_1^0 represent the stable and unstable time evolution of left mechanical mode, respectively, after the critical point λ_c, in arbitrary unites. (d) Transverse Lyapunov exponents (TLEs) versus the coupling parameter λ, where the blue solid curves correspond to the two largest TLEs and the black dashed line indicates the largest TLE of the unstable state after the transition. The pink and light blue backgrounds correspond to synchronized and antiphase synchronized states, respectively.

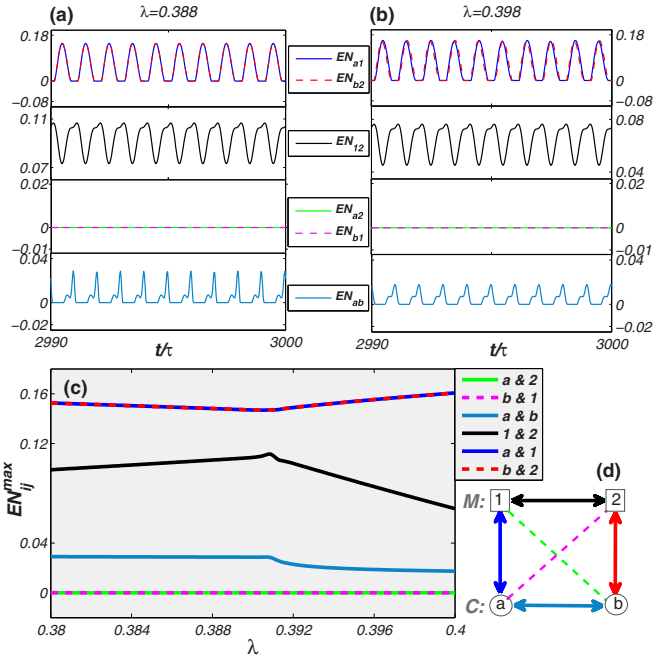

FIG. 4. (Color online) (a) and (b) Time evolution of the measure of quantum entanglement between the optical and mechanical modes for $\lambda = 0.388$ and 0.398, respectively. (c) Maximum quantum entanglement measure (maximum logarithmic negativity) versus λ. (d) Illustration of quantum entanglement between different modes in the two cavities, where, respectively, "M" and "C" stand for mechanical and optical cavity modes, indices "1" and "2" denote the mechanical modes from the left and the right subsystems, and "a" and "b" represent the optical modes in the left and the right cavities. The solid arrows mean there are quantum entanglement between the two modes with colors corresponding to those in (a) and (b). The dashed lines indicate lack of quantum entanglement.

covariance matrix can be expressed as

$$V = [V_{ij}]_{8\times 8} = \begin{bmatrix} I_1 & C_{1a} & C_{12} & C_{1b} \\ C_{a1} & I_a & C_{a2} & C_{ab} \\ C_{21} & C_{2a} & I_2 & C_{2b} \\ C_{b1} & C_{ba} & C_{b2} & I_b \end{bmatrix}, \quad (6)$$

where I_i and C_{ij} are 2×2 matrices and $C_{ij} = C_{ji}^T$. Thus, the covariance matrix for two entangled modes is given by

$$v_{ij} = \begin{bmatrix} I_i & C_{ij} \\ C_{ij}^T & I_j \end{bmatrix}, \quad (7)$$

where $I_{i,j}$ and C_{ij} are 2×2 matrices. For convenience, we use the indices $(i,j) = (1,2)$ and $(i,j) = (a,b)$ to specify the mechanical and optical modes, respectively, for the left and right side subsystems. For example, "1b" denotes the entanglement between the mechanical mode on the left side and the optical mode on the right side, and "$a2$" denotes the entanglement between the optical mode on the left side and the mechanical model on the right side, and so on. The LN value between any two modes is given by

$$EN_{ij} = \max[0, -\ln(2\eta_{ij}^-)], \quad (8)$$

where $\eta_{ij}^- = \sqrt{\Sigma_{ij} - [\Sigma_{ij}^2 - 4|v_{ij}|]^{1/2}}/\sqrt{2}$ and $\Sigma_{ij} = |I_i| + |I_j| - 2|C_{ij}|$. Physically meaningful LN values fall in the unit interval $[0,1]$, where zero means absence of any degree of entanglement and the unity value indicates perfect entanglement. Negative LN values may appear in the calculations, which are physically meaningless. In this case, the actual values are zero.

Note that, in calculating the logarithmic negativity, the quantum steady state for the fluctuations should be a zero-mean, bipartite Gaussian process [31]. To validate this method, we repeatedly solve Eq. (1) with noise terms by using the second-order Heun method [32] and find that all fluctuations about the steady oscillation exhibit a Gaussian distribution.

Figures 4(a) and 4(b) show the time evolution of the various LN measures for $\lambda = 0.388$ and 0.398, respectively. We see that there is strong entanglement between the mechanical and optical modes in the same cavity, and cross-cavity entanglement occurs only between modes of the same nature. That is, there is no entanglement between the mechanical (optical) mode in the left cavity and the optical (mechanical) mode in the right cavity. These results indicate that, in

general, entanglement is much stronger between modes in the same cavity than those across the cavities. To provide further support, we show in Fig. 4(c) the maximum LN values associated with four different pairs of modes: $1a$, $2b$, 12, and ab, as functions of the intercavity coupling parameter λ about the transition point, where the values associated with the pairs $1a$ and $2b$ are identical due to symmetry.

The remarkable phenomenon is the occurrence of a "cusp" type of behavior in all four functions at the transition point where the derivatives of the functions are not continuous. This is characteristic of second-order phase transition. Especially, the situation considered is optical coupling between the two cavities. Due to the intracavity coupling between the optical and mechanical modes, there is a considerable amount of quantum entanglement between the mechanical modes in the two cavities. As the intercavity coupling is strengthened towards the transition point in which the classical dynamics is in-phase synchronization, the degree of entanglement between the mechanical modes increases. But after the transition, classical antiphase synchronization sets in, and this leads to a decrease in the degree of entanglement between the mechanical modes in the two subsystems.

Such a cusp type of catastrophe in quantum entanglement between two identical subsystems is remarkably similar to quantum phase transition (QPT) in the Dicke model [33], where the Hamiltonian contains a nonlinear coupling between the bosonic mode and an ensemble of two-level atoms. In our optomechanical system the two identical subsystems are linearly coupled. Despite the difference in the nature of the coupling, QPT in the Dicke model can provide insights into the cusp behavior in our system. In particular, in the Dicke model, the divergent behavior in quantum entanglement is similar to the quantum cusp catastrophe about the corresponding bifurcation point and the Dicke Hamiltonian also has a classical cusp singularity [20,33]. In our coupled system, in the classical limit, the transition can be characterized as a Hopf-like bifurcation, which is not singular. In the quantum regime, the transition is associated with changes in the phonon number and in the Wigner density due to the emergence of self-induced oscillations [34]. In the whole parameter range studied, there is a common background state driven by the modulated laser, which induces quantum entanglement between the two subsystems. As the coupling strength is increased towards the critical point, a new state emerges, leading to characteristic changes in the quantum entanglement measure. As a result, a second-order, cusp type of phase transition in quantum entanglement occurs.

The transition point can be modulated by changing the amplitude E_1 of the driving laser for the optomechanical subsystems, as shown in Fig. 5(a). As E_1 is increased, the maximum values of LN also increase, signifying stronger entanglement between the two cavities. For the special case of $E_1 = 0$, before the transition the classical dynamics reaches a steady state with little quantum entanglement, but the antiphase synchronization state sets in at some critical point of the intercavity coupling parameter. In this case, the degree of intercavity entanglement between the optical modes tends to increase after the onset of antiphase synchronization, as shown in Fig. 5(b).

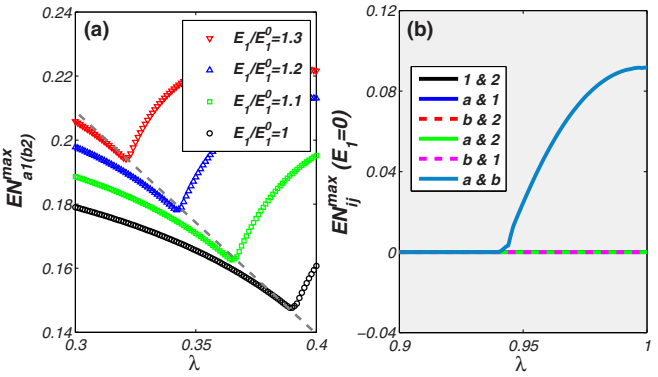

FIG. 5. (Color online) Effect of driving laser power on the transition point: (a) Maximum LN values between the mechanical modes for laser amplitude $E_1 = E_1^0, 1.1E_1^0, 1.2E_1^0, 1.3E_1^0$ (from lower to upper curves), where $E_1^0/\omega_m = 1.351 \times 10^4$. The gray dashed line indicates a linear relation between the critical points λ_c and E_1. (b) Maximum LN values between the optical modes in the two cavities versus λ for $E_1 = 0$.

To summarize, we uncover a transition from in-phase to antiphase synchronization in a system of two optically coupled optomechanical cavities. The emergence of the antiphase synchronization state is shown to be a result of a Hopf bifurcation from an oscillatory state. Calculations of the quantum-entanglement measures for various combinations of the mechanical and optical modes reveal a second-order phase transition type of change at the critical point. In a more general context, our work addresses the fundamental issue of quantum manifestations of transitions among distinct types of collective behaviors in classically complex dynamical systems, an emerging area that deserves further efforts.

This work was supported by AFOSR under Grant No. FA9550-12-1-0095 and by ONR under Grant No. N00014-08-1-0627.

[1] A. M. O. de Almeida, *Hamiltonian Systems: Chaos and Quantization* (Cambridge University Press, Cambridge, 1988); F. Haake, *Quantum Signatures of Chaos*, 3rd ed., Springer series in synergetics (Springer-Verlag, Berlin, 2010).

[2] O. Bohigas, M. J. Giannoni, and C. Schmit, Phys. Rev. Lett. **52**, 1 (1984); M. V. Berry, Proc. R. Soc. London Series A Math. Phys. Eng. Sci. **400**, 229 (1985); M. V. Berry and M. Robnik, J. Phys. A Math. and Gen. **19**, 649 (1986).

[3] S. W. McDonald and A. N. Kaufman, Phys. Rev. Lett. **42**, 1189 (1979); Phys. Rev. A **37**, 3067 (1988); E. J. Heller, Phys. Rev. Lett. **53**, 1515 (1984); E. B. Bogomolny, Physica D **31**, 169 (1988); R. L. Waterland, J. M. Yuan, C. C. Martens, R. E. Gillilan, and W. P. Reinhardt, Phys. Rev. Lett. **61**, 2733 (1988);

M. V. Berry, Proc. R. Soc. London Series A Math. Phys. Eng. Sci. **423**, 219 (1989).

[4] R. Blümel and U. Smilansky, Phys. Rev. Lett. **60**, 477 (1988); Physica D **36**, 111 (1989); R. A. Jalabert, H. U. Baranger, and A. D. Stone, Phys. Rev. Lett. **65**, 2442 (1990); C. M. Marcus, A. J. Rimberg, R. M. Westervelt, P. F. Hopkins, and A. C. Gossard, *ibid.* **69**, 506 (1992); Y.-C. Lai, R. Blümel, E. Ott, and C. Grebogi, *ibid.* **68**, 3491 (1992); R. Ketzmerick, Phys. Rev. B **54**, 10841 (1996).

[5] S. Strogatz, *The Emerging Science of Spontaneous Order* (Hyperion, New York, 2003); H. Fujisaka and T. Yamada, Prog. Theo. Phys. **69**, 32 (1983); L. M. Pecora and T. L. Carroll, Phys. Rev. Lett. **64**, 821 (1990); M. Barahona and L. M. Pecora, *ibid.* **89**, 054101 (2002); T. Nishikawa, A. E. Motter, Y.-C. Lai, and F. C. Hoppensteadt, *ibid.* **91**, 014101 (2003).

[6] L.-Y. Cao and Y.-C. Lai, Phys. Rev. E **58**, 382 (1998); M.-C. Ho, Y.-C. Hung, and C.-H. Chou, Phys. Lett. A **296**, 43 (2002); W. Liu, J. Xiao, X. Qian, and J. Yang, Phys. Rev. E **73**, 057203 (2006); Q. Chen, Y.-C. Lai, J. Chae, and Y. Do, Phys. Rev. B **87**, 144304 (2013).

[7] M. Zalalutdinov, K. Aubin, M. Pandey, A. Zehnder, R. Rand, H. Craighead, J. Parpia, and B. Houston, Appl. Phys. Lett. **83**, 3281 (2003); S. Kaka, M. R. Pufall, W. H. Rippard, T. J. Silva, S. E. Russek, and J. A. Katine, Nature (London) **437**, 389 (2005); F. Mancoff, N. Rizzo, B. Engel, and S. Tehrani, *ibid.* **437**, 393 (2005); M. Li, H. Tang, and M. Roukes, Nature Nanotech. **2**, 114 (2007); M. Bagheri, M. Poot, M. Li, W. P. H. Pernice, and H. Tang, *ibid.* **6**, 726 (2011).

[8] S.-B. Shim, M. Imboden, and P. Mohanty, Science **316**, 95 (2007).

[9] C. A. Holmes, C. P. Meaney, and G. J. Milburn, Phys. Rev. E **85**, 066203 (2012).

[10] M. Zhang, G. S. Wiederhecker, S. Manipatruni, A. Barnard, P. McEuen, and M. Lipson, Phys. Rev. Lett. **109**, 233906 (2012).

[11] F. Massel, S. U. Cho, J.-M. Pirkkalainen, P. J. Hakonen, T. T. Heikkilä, and M. A. Sillanpää, Nat. Commun. **3**, 987 (2012); A. Tomadin, S. Diehl, M. D. Lukin, P. Rabl, and P. Zoller, Phys. Rev. A **86**, 033821 (2012).

[12] O. V. Zhirov and D. L. Shepelyansky, Eur. Phys. J. D **38**, 375 (2006).

[13] O. V. Zhirov and D. L. Shepelyansky, Phys. Rev. B **80**, 014519 (2009).

[14] T. E. Lee and H. R. Sadeghpour, Phys. Rev. Lett. **111**, 234101 (2013).

[15] T. E. Lee and M. C. Cross, Phys. Rev. A **88**, 013834 (2013).

[16] M. Ludwig and F. Marquardt, Phys. Rev. Lett. **111**, 073603 (2013).

[17] T. E. Lee, C.-K. Chan, and S. Wang, Phys. Rev. E **89**, 022913 (2014).

[18] T. J. Kippenberg and K. J. Vahala, Science **321**, 1172 (2008); M. Li, W. H. P. Pernice, C. Xiong, T. Baehr-Jones, M. Hochberg, and H. X. Tang, Nature (London) **456**, 480 (2009); F. Marquardt and S. M. Girvin, Physics **2**, 40 (2009); S. Grblacher, J. B. Hertzberg, M. R. Vanner, G. D. Cole, S. Gigan, K. C. Schwab, and M. Aspelmeyer, Nature Physics **5**, 485 (2009); A. Schliesser, O. Arcizet, R. Riviére, G. Anetsberger, and T. J. Kippenberg, *ibid.* **5**, 509 (2009); G. Anetsberger, O. Arcizet, Q. P. Unterreithmeier, R. Riviére, A. Schliesser, E. M. Weig, J. P. Kotthaus, and T. J. Kippenberg, *ibid.* **5**, 909 (2009); P. Verlot, A. Tavernarakis, T. Briant, P.-F. Cohadon, and A. Heidmann, Phys. Rev. Lett. **102**, 103601 (2009); J. D. Teufel, T. Donner, M. A. Castellanos-Beltran, J. W. Harlow, and K. W. Lehnert, Nat. Nanotech. **4**, 820 (2009); M. Li, W. H. P. Pernice, and H. X. Tang, Nat. Photon. **3**, 464 (2009); D. E. Chang, A. H. Safavi-Naeini, M. Hafezi, and O. Painter, New J. Phys. **13**, 023003 (2011); G. Heinrich, M. Ludwig, J. Qian, B. Kubala, and F. Marquardt, Phys. Rev. Lett. **107**, 043603 (2011).

[19] M. Aspelmeyer, T. J. Kippenberg, and F. Marquardt, arXiv:1303.0733 (2013).

[20] G. Wang, L. Huang, Y.-C. Lai, and C. Grebogi, Phys. Rev. Lett. **112**, 110406 (2014).

[21] M. Eichenfield, R. Camacho, J. Chan, K. J. Vahala, and O. Painter, Nature (London) **459**, 550 (2009).

[22] M. Eichenfield, J. Chan, R. M. Camacho, K. J. Vahala, and O. Painter, Nature (London) **462**, 78 (2009).

[23] J. D. Teufel, T. Donner, D. Li, J. W. Harlow, M. S. Allman, K. Cicak, A. J. Sirois, J. D. Whittaker, K. W. Lehnert, and R. W. Simmonds, Nature (London) **475**, 359 (2011); A. H. Safavi-Naeini, J. Chan, J. T. Hill, Thiago P. Mayer Alegre, A. Krause, and O. Painter, Phys. Rev. Lett. **108**, 033602 (2012).

[24] C. Joshi, J. Larson, M. Jonson, E. Andersson, and P. Öhberg, Phys. Rev. A **85**, 033805 (2012).

[25] B. Peng, Åžahin Kaya Ã–zdemir, F. Lei, F. Monifi, M. Gianfreda, G. L. Long, S. Fan, F. Nori, C. M. Bender, and L. Yang, Nature Physics **10**, 394 (2014).

[26] D. F. Walls and G. J. Milburn, *Quantum Optics* (Springer, Berlin, 1994).

[27] V. Giovannetti and D. Vitali, Phys. Rev. A **63**, 023812 (2001).

[28] A. Mari and J. Eisert, Phys. Rev. Lett. **103**, 213603 (2009).

[29] L. M. Pecora and T. L. Carroll, Phys. Rev. Lett. **80**, 2109 (1998).

[30] G. Adesso and F. Illuminati, J. Phys. A **40**, 7821 (2007).

[31] D. Vitali, S. Gigan, A. Ferreira, H. R. Böhm, P. Tombesi, A. Guerreiro, V. Vedral, A. Zeilinger, and M. Aspelmeyer, Phys. Rev. Lett. **98**, 030405 (2007).

[32] C. Van den Broeck, J. M. R. Parrondo, R. Toral, and R. Kawai, Phys. Rev. E **55**, 4084 (1997).

[33] C. Emary and T. Brandes, Phys. Rev. E **67**, 066203 (2003); N. Lambert, C. Emary, and T. Brandes, Phys. Rev. Lett. **92**, 073602 (2004); C. Emary, N. Lambert, and T. Brandes, Phys. Rev. A **71**, 062302 (2005).

[34] J. Qian, A. A. Clerk, K. Hammerer, and F. Marquardt, Phys. Rev. Lett. **109**, 253601 (2012).